Earth Surf. Dynam., 5, 199–209, 2017
www.earth-surf-dynam.net/5/199/2017/
doi:10.5194/esurf-5-199-2017

Earth Surface Dynamics
Open Access
EGU

A new CT scan methodology to characterize a small aggregation gravel clast contained in a soft sediment matrix

Laurent Fouinat[1], Pierre Sabatier[1], Jérôme Poulenard[1], Jean-Louis Reyss[2], Xavier Montet[3], and Fabien Arnaud[1]

[1]EDYTEM, Université Savoie Mont Blanc, CNRS 73376 Le Bourget du Lac CEDEX, France
[2]LSCE, Université de Versailles Saint-Quentin CEA-CNRS, Avenue de la Terrasse, 91198 Gif-sur-Yvette CEDEX, France
[3]University of Geneva Department of Radiology and Medical Informatics Genève, Rue Gabrielle-Perret-Gentil 4, C1211, Geneva, Switzerland

Correspondence to: Laurent Fouinat (laurent.fouinat@univ-smb.fr)

Received: 20 April 2016 – Discussion started: 13 May 2016
Revised: 13 January 2017 – Accepted: 8 February 2017 – Published: 28 March 2017

Abstract. Over the past decades, X-ray computed tomography (CT) has been increasingly applied in the geosciences community. CT scanning is a rapid, non-destructive method allowing the assessment of relative density of clasts in natural archives samples. This study focuses on the use of this method to explore instantaneous deposits as major contributors to sedimentation of high-elevation lakes in the Alps, such as the Lake Lauvitel system (western French Alps). This lake is located within a very steep valley prone to episodic flooding and features gullies ending in the lake. This variety of erosion processes leads to deposition of sedimentary layers with distinct clastic properties. We identified 18 turbidites and 15 layers of poorly sorted fine sediment associated with the presence of gravels since AD 1880. These deposits are respectively interpreted as being induced by flood and wet avalanche. This constitutes a valuable record from a region where few historical records exist. This CT scan approach is suitable for instantaneous deposit identification to reconstruct past evolution and may be applicable to a wider variety of sedimentary archives alongside existing approaches.

1 Introduction

At their introduction to the field around 50 years ago, X-ray radiographs were initially used to explore the internal structure of sediment cores (Bouma, 1964; Baker and Friedman, 1969) in order to optimize the opening process or even explore bioturbation structures in the sediment (Howard, 1968). One of the technical problems was the loss of information with respect to depth, as the radiographs are a planar representation of a 3-D structure. A recent review of computed tomography (CT) scans in the geosciences (Cnudde and Boone, 2013) demonstrates the growing application possibilities of X-ray technology as well as the limits of the technique. Improvements in CT scanning allowed exploration of complex sedimentary structures through 3-D reconstructions, leading to improvement compared to classic 2-D imaging (Pirlet et al., 2010; Bendle et al., 2015). The method is based on the relative density of each voxel (i.e., volumetric pixel) constituting the chosen sample. The position of each voxel is set on a x, y, z frame allowing association of adjacent identical density voxels to identify sediment constituents. Image analysis of the 3-D numerical model can then be used to obtain quantitative information about selected constituents as well as volumetric information (Bolte and Cordelieres, 2006). This type of methodology was recently used to identify and quantify gypsum formation in marine sediments (Pirlet et al., 2010) as well as different sediment clast deposition in a glacio-lacustrine varved context (Bendle et al., 2015).

High-elevation lakes situated in mountain areas are often characterized by elevated and highly variable sedimen-

tation rates (Arnaud et al., 2016). The variety of erosion processes caused by chemical and mechanical weathering as well as rock breaking by frost action creates heterogeneous grain size elements. Extreme climatological events can trigger several high-energy transport mechanisms which could induce deposition of these elements in lake sediments. Depending on the processes, extreme events may induce different sedimentary structures containing coarse grains (Arnaud et al., 2002; Sletten et al., 2003; Nielsen et al., 2016). Fluvial events such as floods are able to transport very large quantities of sediment in a short period of time (Sturm and Matter, 1978; Jenny et al., 2014). In recent years, they have also been largely identified as a major sedimentary source in high-elevation lakes (Giguet-Covex et al., 2012; Glur et al., 2013; Wilhelm et al., 2013, 2015; Wirth et al., 2013). As floods are formed by heavy precipitation events, the torrential stream transporting sediment in suspension will enter into the lake and create a density current resulting in a characteristic deposit called turbidite (Gilli et al., 2013). The density difference between subaerial flow and lake water can create different underwater flow, but each type will result in a coarse-grain base with a fining-upward trend (Sturm and Matter, 1978). In certain cases, lake surroundings may include gullies orienting subaerial flow into the water. Two mass-wasting types of transport related to these gullies were identified in high-elevation lakes' sediments. The first type is debris flow triggered by water transport but with a lower water content compared to floods (Postma, 1986; Dasgupta, 2003). Its transport capacity is thus increased and they will form specific deposits in underwater environments due to their higher density and sediment cohesion (Mulder and Alexander, 2001). Typical deposits are composed of a load cast layer containing a basal erosive surface, which is overlain by a fining-upward layer comprising the finer sediment fractions (Sletten et al., 2003; Irmler et al., 2006). The second main type of input can be attributed to wet-snow avalanches that occur mostly over springtime. Wet-snow avalanches are typically observed in steep alpine valleys where the slope exceeds 28°, but they have been observed on slopes as low as 15° (Jomelli and Bertran, 2001; Ancey and Bain, 2015). They are capable of transporting sediments ranging in size from fine eolian particles up to cobbles or boulders (van Steijn et al., 1995; Blikra and Nemec, 1998; Jomelli et al., 2007; Sæmundsson et al., 2008; Van Steijn, 2011). Sediment is then carried downslope by rapidly flowing water-saturated snow and deposited directly into lake water or onto the frozen lake surface (Luckman, 1975, 1977). Wet avalanches in lacustrine deposits have been identified by Vasskog et al. (2011) using grain size analysis to identify layers of poorly sorted grain accumulation associated with gravels resulting in a multi-modal grain size distribution. Such deposits on lake ice would result in drop stones at thaw season (Luckman, 1975), and may contain such deposits on lake ice would result in drop stones at thaw season, and may contain terrestrial organic matter (OM; Irmler et al., 2006; Wilhelm et al., 2013; Korup and Rixen, 2014).

All of these high-energy processes led to the presence of coarse-grained deposits, and methods used to identify and count the coarser elements have been based on wet sieving of successive layers of sedimentary cores, which is a both time-consuming and destructive method (Seierstad et al., 2002; Sletten et al., 2003; Nesje et al., 2007; Vasskog et al., 2011). In this study, we propose a complementary method to grain size analysis to better characterize these coarse grains in a simpler, faster and non-destructive way based on the use of CT scanning. This provides an ideal context in which to test our novel X-ray CT based technique and application on sediment cores from Lake Lauvitel located in the Oisans Valley (western French Alps).

2 Materials and methods

2.1 Study site

Lake Lauvitel (44°58′11.4″ N, 6°03′50.5″ E) is located 1500 m above sea level (a.s.l.) in the Oisans Valley of the western French Alps, 35 km southeast of Grenoble. The lake covers an area of 0.35 km^2 and is 61 m deep, and the total drainage area is approximately 15.1 km^2 . The lake was created after a large rockslide dated to 4.7 ± 0.4 kyr ^{10}Be exposure age (Delunel et al., 2010). The natural permeable dam created after this event caused a change in lake level of approximately 20 m. Due to geomorphological settings, slopes around the lake are very steep and three avalanche corridors (C1, C2, and C3) are present on the western side of the lake (Fig. 1b). They are accompanied by the presence of snow accumulation at their bottom in spring (National Park ranger, J. Forêt, personal communication, 2014), and avalanches have been observed in C1 (Fig. 1e). The watershed bedrock consists mainly of granite and gneiss, with minor outcrops of sedimentary rocks (Triassic limestone). The C1 track ends in an upper basin in the northern part of the lake, likely with no connection to the deeper part of the lake. C2 and C3 are located just above the coring location; there is no clear evidence of an obstacle preventing the sediment input from reaching the coring location. From the end of December to the beginning of May, the lake surface is frozen, and snow covers most of the watershed. The lake and its surroundings are situated in the Ecrins National Park restricted area.

2.2 Core description and methods

The core LAU11P2 (76 cm) was retrieved using a short UWITEC gravity corer to obtain a well-preserved interface, and LAU1104A (104.5 cm) was retrieved using a piston corer with a 90 mm sampling tube at the same location. The cores were split lengthwise and photographed at high resolution (20 pixels mm^{-1}). We examined in detail the visual macro-

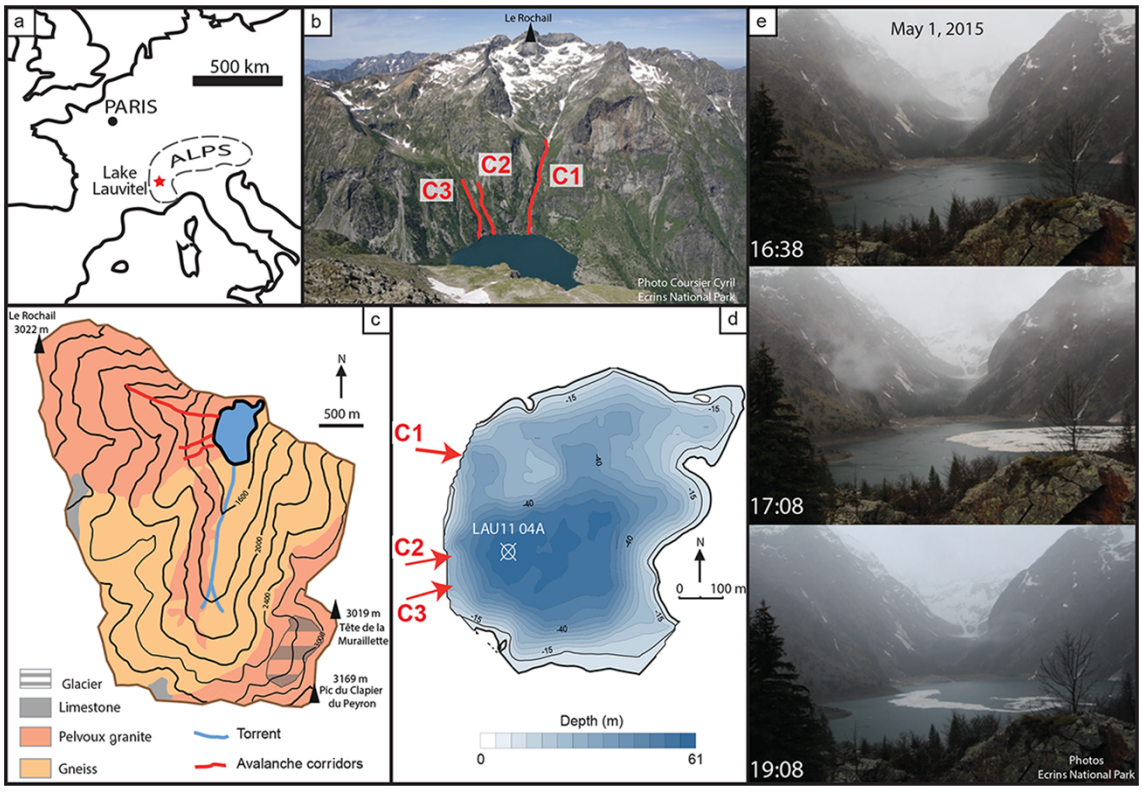

Figure 1. **(a)** Location of Lake Lauvitel. **(b)** Photo looking westward toward the location of the three avalanche corridors in the Lake Lauvitel watershed. **(c)** Simplified geologic map of the Lake Lauvitel watershed. **(d)** Lake Lauvitel bathymetric map and location of the three avalanche corridors and position of the LAU1104A coring point. **(e)** Photos of the lake looking to the south, with an avalanche entering the lake via the C1 corridor on 1 May 2015.

scopic features of each core to define the different sedimentary facies to determine the stratigraphic correlation between the two cores.

CT scanning was performed at Hopitaux Universitaires de Genève (HUG) using a multidetector CT scanner (Discovery 750 HD, GE Healthcare, Milwaukee, WI, USA). The acquisition parameters were set as follows: 0.6 s gantry rotation time, 100 kVp, 0.984:1 beam pitch, 40 mm table feed per gantry rotation, and a z-axis tube current modulation with a noise index (NI) of 28 (min/max mA, 100/500) and a 64×0.625 mm detector configuration. All CT acquisitions were reconstructed with the soft tissue and bone kernel in order to enhance the density contrast (Tins, 2010). The images reconstructed with the bone kernel were used for subsequent analysis. The raw DICOMM images were converted to an 8 bit TIFF format using Weasis (v2.0.3) viewer. The radiograph resolution is 512×512 pixels, with up to 256 greyscale values. In this study, the sediment core was divided into 1045 frames each 1 mm thick, with each pixel corresponding to a resolution of up to 500×500 µm and thus a voxel of 0.25 mm^3. The images were then stacked using the Image J FIJI application, and image treatments were performed using the 3-D Object Counter plugin (Bolte and Cordelieres, 2006). First, we set a threshold to isolate the selected grey values, and we then applied a despeckle filter to remove the noise due to measurement. Finally, 3-D Object Counter was used to reconstruct the particles and characterize them in a 3-D coordinate system.

Grain size measurements were carried out on the core using a Malvern Mastersizer 800 particle sizer at a lithology dependent sampling interval. Ultrasonics were used to dissociate particles and to avoid flocculation. Several layers of gravel-sized mineralogic particles were identified (Fig. 2a) in the LAU1104 sediment core. To obtain a quantitative estimate of these particles, we passed samples through a 1 mm mesh and wet-sieved the sediment at variable intervals from 1 to 3 cm depending on the gravel concentration. The number of particles > 2 mm and macro-remains present in the sieve was counted for each interval in the core LAU1104A.

The chronology of the Lake Lauvitel sediment sequence is based on short-lived radionuclide measurements. The short-lived radionuclides in the upper 75 cm of core LAU11P2 were measured using high-efficiency, very low background, well-type Ge detectors at the Modane Underground Laboratory (LSM; Reyss et al., 1995). The sampling intervals followed facies boundaries, resulting in a non-regular sam-

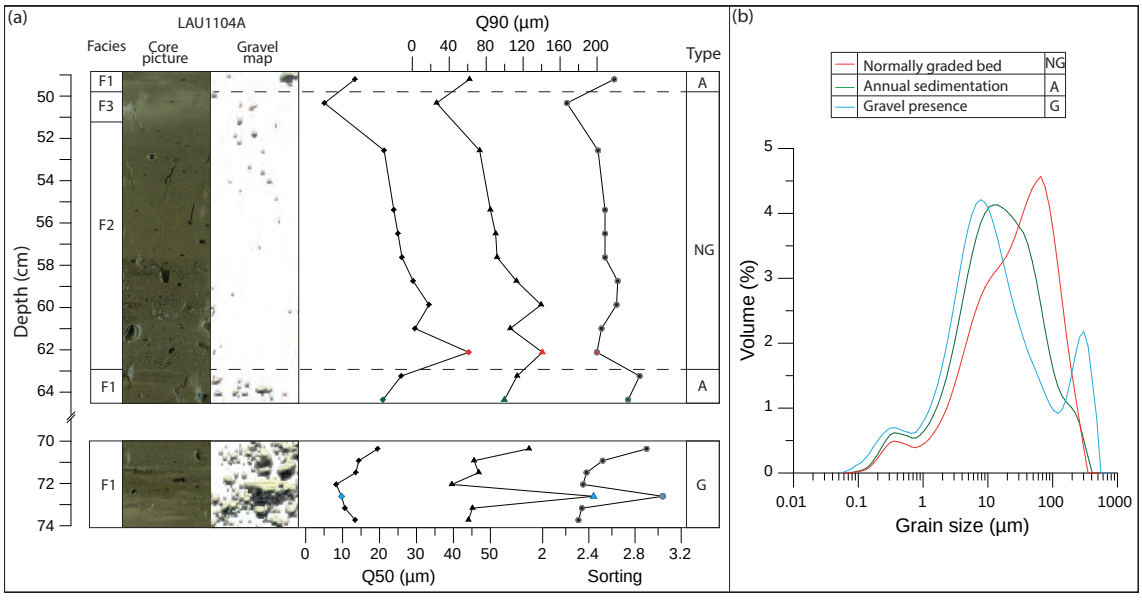

Figure 2. **(a)** Characterization of typical facies of LAU1104A sediment core, based on median grain size (Q50), 10th percentile coarse grains (Q90) and sorting parameters. **(b)** Comparison between NG, normally graded bed base sample (red line); A, annual sedimentation (green line); and G, gravel presence (blue line) grain size distributions.

pling of approximately 1 cm. Twelve thick beds (at depths of 10.4–12.7, 17.3–19, 22.9–24.8, 29.7–30.9, 38–39, 40.6–42.4, 43.1–44.2, 45.7–50, 54.5–56.9, 60.4–62.5, 64.1–66 and 67.2–68.3 cm) were not analyzed because they were considered to be instantaneous deposits or part of an instantaneous deposit (see Results). ^{210}Pb excess was calculated as the difference between total ^{210}Pb and ^{226}Ra activities.

3 Results

3.1 Lithostratigraphy

The core lithology is composed of three facies (Fig. 2a). Facies 1 (F1) is silty-clay, dark-brown, finely laminated layer. It is interbedded by two other facies that are almost always associated with each other: facies 2 (F2) is a normally graded bed from coarse sand to silt, sometimes with an erosive base; this facies is always associated with a thin white clay-rich layer, facies 3 (F3), on the top. Figure 2b presents typical normally graded beds with grain size distribution (in red) characterized by a median grain size (Q50) of 44.1 and a mode of 81 µm. F1 (in green) exhibits a median grain size of 13.5 and a mode of 11.9 µm. Sometimes, F1 presence coincides with coarse gravel in the sediment; thus, the median grain size is similar 9.7 µm, but two modes are discernible at 7.2 and 258 µm. The sorting parameter reveals different values depending on the deposit type: 2.50 on average in the normally graded beds, 2.65 for the annual sedimentation and 3.05 for annual sedimentation with gravel presence. The small Q50 difference between annual sedimentation with and without gravel supposes limited addition in the fine grains fractions. At the same time, the fraction over 100 µm and poor sorting and Q90 reveal a significant addition of sand size grains in the gravel layers. The presence of terrestrial macro-remains is sometimes identifiable in F2. A total of 18 normally graded beds are present in the core LAU1104A, with thicknesses ranging from 0.7 to 13 cm. We also identified 15 layers with poorly sorted fine sediment associated with gravel presence, with thicknesses ranging from 0.3 to 5.9 cm.

The CT scan analysis is based on relative density expressed on the histogram (Fig. 3a) representing the frequency of each of 1–255 levels of grey (0 is not shown on the graph due to overrepresentation corresponding to the background signal). Three modes representing the most frequent values are apparent in the histogram and are associated with certain types of sediment. The first mode is centered on the 106 value. After selecting this mode, we isolated the numerical values in order to map them by using the plugin. The corresponding elements in the sediment core were small OM macroremains such as a *Pinus* twig found at 58 cm depth (Fig. 3e1). We thus selected the 95–125 range to identify OM. The second mode, centered on the 174 value, is relatively denser than OM. Its larger spectrum and high count values correspond to the most common element in the sediment core, which would be the silty clay sedimentation matrix (Fig. 3b). The last mode is essentially the 255 level of grey. It is the densest value possible, thus corresponding to denser elements present in the silty-clay matrix. We selected the 250–255 value range and isolated them, and then searched for corresponding particles in the sediment core.

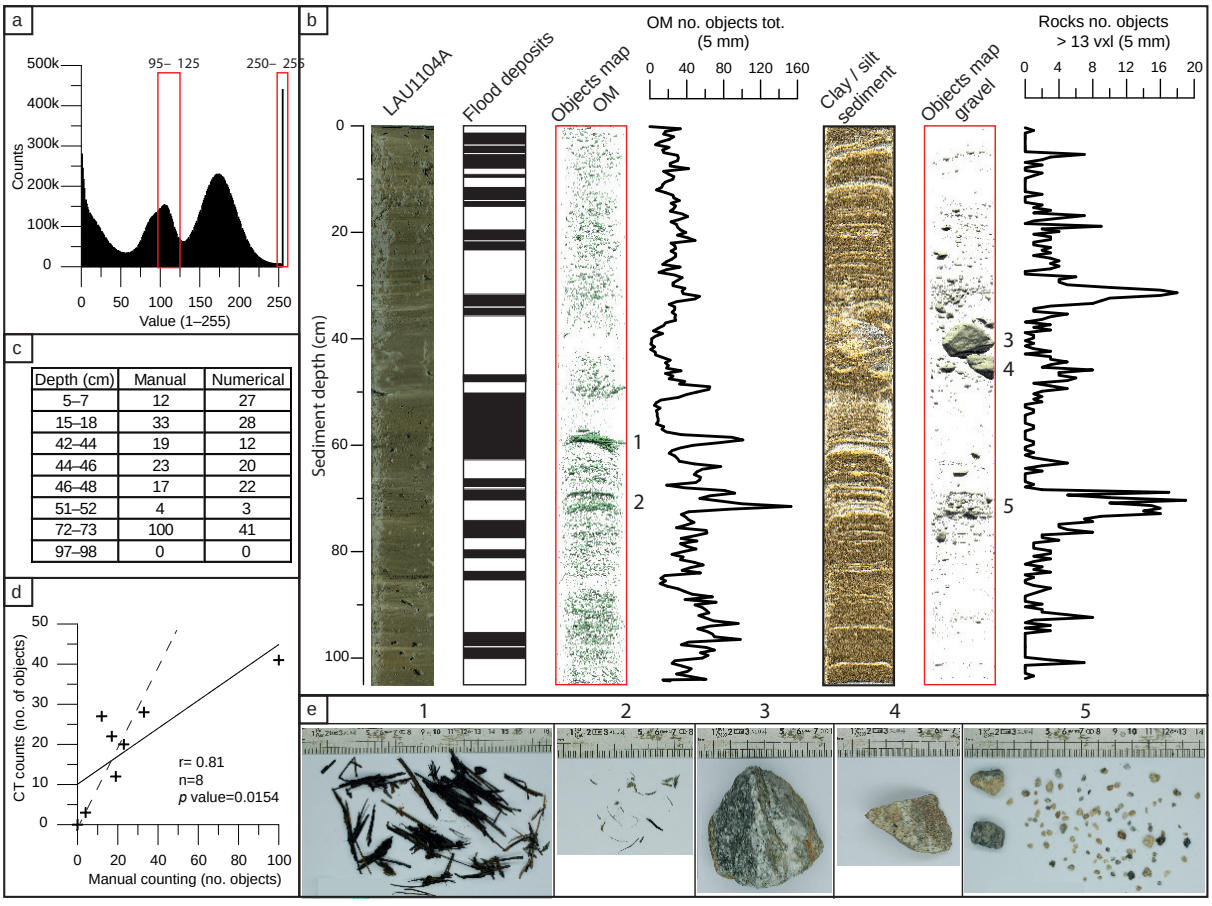

Figure 3. **(a)** Number of counts histogram for 1 to 255 levels of grey; selected range for OM (95–125) and for gravels (240–255) shown in red. **(b)** From left to right: core LAU1104A photography, position of flood deposits, CT image stacks of both rocks and OM and corresponding totals summed at 5 mm intervals. **(c)** Selected depth for comparison between manual and numerical counts in core LAU1104A. **(d)** Correlation between manual and numerical rock counts (solid line); CT counts: manual counts (dashed line). **(e)** Photographs of organic matter (e1, e2) and gravel-sized elements (e3, e4, e5) recovered from the LAU1104 sediment core.

Wet sieving allowed identification of gravel-sized granite elements in the sediment core (Fig. 3e3–e4).

To compare objects counted numerically and objects counted manually, we need to know the size limit in units of volume (voxels), which is equivalent to 2 mm diameter holes in a sieve. In 2-D, a particle is retained in the sieve only if at least two sides are 2 mm in length, meaning at least two sides are 4 pixels long. Therefore, a particle of 16 (4×4) pixels with four sides that are 2 mm long will be retained in the sieve. However, if the same particle is missing one corner (minus 3 pixels, corresponding to a particle of 13 pixels), the particle would still be large enough to be retained in the sieve. This angular shape is more likely to be encountered in avalanche deposits. Consequently, we set the size limit of the 3-D Object Counter plugin to 13 pixels, which corresponds to 13 voxels. The organic macroremains are composed of herbs, twigs or even roots, and their shapes were very complicated. Therefore, we did not choose any volume limit in their identification process.

In the LAU1104A sediment core, a total of 456 gravel clasts equal to or larger than 13 voxels were identified for a total of 112 683 mm^3. The largest high-density object recovered from the core LAU1104A was an angular piece of granite of over 6 cm on its longest side and weighing 206.03 g. Considering the weight of the water displaced by the fully immersed, its actual volume can be calculated at 79 310 mm^3. In comparison, the numerical volume is estimated to be 376 187 voxels, corresponding to 89 690 mm^3. A difference of +11.6 % in the volume for the CT counting is observed which is probably due to pixel resolution. The volume is slightly overestimated but still close to the actual rock volume.

We then compared the 3-D Object Counter results and the coarse grains recovered from the sediment cores in slices of variable thickness ranging from 1 to 3 cm. The depth 97–98 cm had no gravel > 2 mm in either the manual or numerical counting (Fig. 3b, d). When considering a large amount of gravel, the manual and numerical counting methods showed

differences. For depths 15–18, 42–44, 44–46, 51–52, and 72–73 cm, the number of gravel clasts was always underestimated by the numerical counting. As the 3-D Object Counter plugin is identifying objects from one pixel and its eight neighbors in 2-D and its 26 neighbors in 3-D (Bolte and Cordelieres, 2006), the identification of objects could vary especially because of the noise treatment and when the object size is close to the image resolution. The numerical counting result is slightly underestimated compared to the manual counting result (30 % on average). However, depths 5–7 and 46–48 cm showed an overestimation by the numerical counting (77 % on average). Considering the resolution, it is possible that a certain number of aggregated sand grains could have been considered gravel by the numerical counting method, leading to an overestimation. This could be explained by the presence of flood deposits in these two depths (Fig. 3b). Aggregated sand-sized elements would be considered by numerical counting as larger elements. In addition, the sand-sized elements are rounder and would go through the sieve, as opposed to an angular particle of similar volume which would be retained in the sieve. Overall, from this comparison between the numerical and the manual counting and accounting for the previously mentioned CT scan bias, we obtained a relatively well constrained positive correlation ($r = 0.81$, $n = 8$; p value $= 0.0154$; Fig. 3d). This correlation remains still satisfactory without the outlier point corresponding to 72–73 cm of depth ($r = 0.78$, $n = 7$; p value $= 0.0038$).

The OM counting identified 7413 objects, spread throughout almost every part of the sediment core. The largest OM element found in the core was 6949 voxels in size, corresponding to 1732 mm^3. This OM element was situated at a depth of 58 cm in the middle of a flood deposit (Fig. 3b) and was identified as a *Pinus* tree twig (Fig. 3e1). In total, 89.2 % of the numerically counted OM elements are under 3.25 mm^3 (13 voxels), and almost every element recovered in the sieve corresponded to small leafs, roots, twigs or herb macroremains (Fig. 3e2).

3.2 Chronology

The ^{210}Pb excess profile (Fig. 4) showed a regular decrease punctuated by drops in $^{210}Pb_{ex}$ activities. Following (Arnaud et al., 2002), these low values of $^{210}Pb_{ex}$ were excluded to construct a synthetic sedimentary record, because these values are related to F2/F3 facies association, which is considered to be composed of instantaneous turbidite deposits. Plotted on a logarithmic scale, the $^{210}Pb_{ex}$ activities revealed a linear trend (Wilhelm et al., 2012). Applying the CFCS model (Goldberg, 1963), we obtain a mean accumulation rate of 3.7 ± 0.3 mm yr^{-1}. The uncertainty in the sedimentation rate was derived from the standard error of the CFCS model linear regression. Ages were then calculated using the CFCS model applied to the original sediment sequence to provide a continuous age–depth relationship. In addition, ^{137}Cs and ^{241}Am activity profiles present two peaks and one peak, respectively. The older peak in ^{137}Cs activity at 28.1 cm is contemporary with the peak in ^{241}Am activity, allowing us to associate it with the peak of nuclear weapons testing in the northern hemisphere in AD 1963. The younger peak in ^{137}Cs activity at 17.3 cm can be attributed to fallout from the Chernobyl accident in AD 1986 (Appleby et al., 1991). These two artificial peaks are in good agreement with the CFCS model (Fig. 4). In addition, we compared the historical flood calendar from the Vénéon river valley from the RTM-ONF database (http://rtm-onf.ifn.fr/) to the instantaneous deposits recovered from the lake sediment for the last 100 years. In local archives, eight major flood events occurred in AD 2008, 2003, 1987, 1962, 1955, 1938, 1922 and 1914, could be correlated to the most important and recent graded deposits at depths of 0.4–2.9, 9.9–11.4, 18.7–20.1, 28.5–32.9, 38.2–39.6, 46–61, 64.9–66.7, and 67.7–69.1 cm, respectively. The good agreement between these independent chronological markers and the $^{210}Pb_{ex}$ ages strongly supports our age–depth model for the last century and validates our interpretation that the F2/F3 facies correspond to instantaneous flood deposits.

4 Discussion

A number of distinct layers, including normally graded beds, are identified in the Lake Lauvitel sedimentary record. Analysis of median grain size (Q50) and the coarser 10th percentile (Q90) parameters from within graded beds leads us to consider these to be turbidites caused by heavy rainfall in the watershed (Støren et al., 2010; Giguet-Covex et al., 2012; Wilhelm et al., 2012, 2013, 2015; Gilli et al., 2013). Gravels were found in the upper part of the flood deposit that are associated with receding torrential activity (Gilli et al., 2013). These gravels are unlikely to have originated from the torrential activity due to the distance from the delta. The presence of gravel in the turbidites could possibly be attributed to debris flow activity resulting in an dense cohesive underflow transforming in a turbidite layer (Weirich, 1988). However, we do not observe a load clast at the base of the deposit as is typical of what a debris flow would exhibit, but instead our results show sparse gravel presence in the upper part of the deposits (Fig. 2). Gravels within flood deposits could be linked to temporary tributaries only active during heavy precipitation, for example flows transmitted through avalanche corridors over summer. A similar pattern of gravel distribution is also observed in the homogeneous fine annual sedimentation (Fig. 2). In these layers, the sorting is similar to that of the annual sedimentation without gravel. This could be explained by the gravel elements falling either directly into the lake or onto the frozen lake surface and subsequently producing drop stones as it melts away.

Fifteen layers are identified exhibiting a high proportion of gravel elements accompanied by poorly sorted fine grains

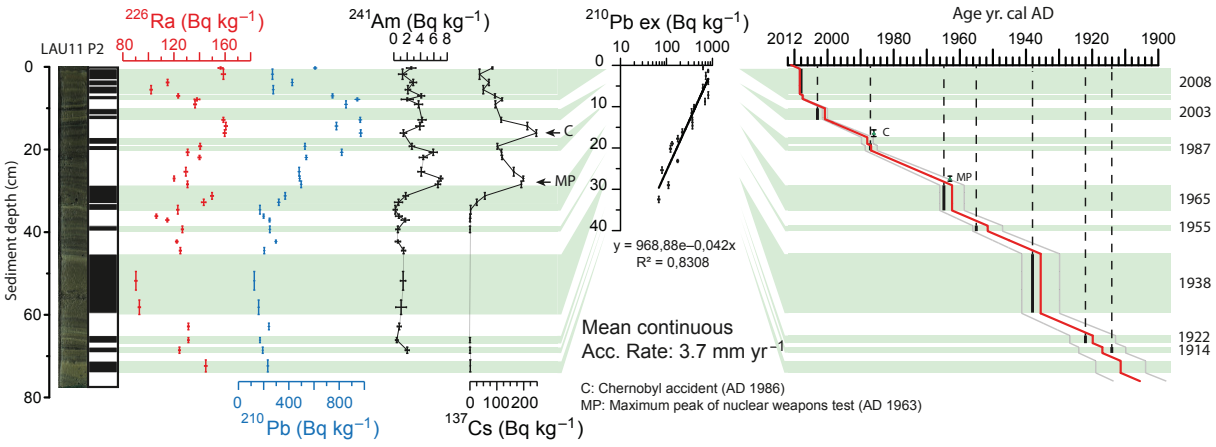

Figure 4. ^{226}Ra, ^{210}Pb, ^{241}Am, and ^{137}Cs activity profiles for core LAU11P2. Application of the CFCS model to the synthetic sedimentary profile of excess ^{210}Pb (without normally graded beds, which are considered to be instantaneous deposits). Resulting age–depth relationship with 1σ uncertainties and indications of historic flood dates associated with normally graded beds and the two artificial radionuclide markers.

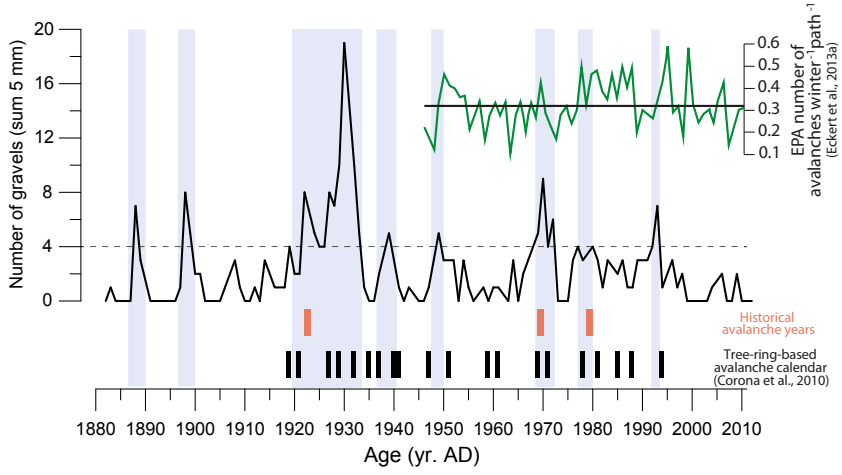

Figure 5. Sum of gravels > 13 voxels at 5 mm intervals identified in the LAU1104A sediment core since AD 1880 without the normally graded beds. The dashed line represents the threshold number from which avalanche periods are identified (highlighted in blue). Exceptional winters found in the bibliography are represented in red (Allix, 1923; Jail, 1970; Ecrins National Park internal report, 1978). EPA (Enquête Permanente sur les Avalanches) number of avalanches per path since AD 1950 is in green, and interannual mean value is in black (Eckert et al., 2013). The avalanche record for the past century is from tree rings in the nearby Romanche river valley (Corona et al., 2010).

of multi-modal grain size distribution (Fig. 2). Similar features have also been observed in Norway, where they are attributed to avalanche induced depositions (Blikra and Nemec, 1998; Seierstad et al., 2002; Nesje et al., 2007; Vasskog et al., 2011). Wet avalanches occur in spring, when warmer temperatures lead to a loss of cohesion and instability in the snowpack. Given that the lake ice does not thaw until late spring, avalanches could either be deposited on ice or enter directly in the water as observed during the 1 May 2015 avalanche (Fig. 1). During this event, the snow flow originated from the C1 corridor in the northern part of the lake containing the upper basin and was thus unlikely to have any sedimentary connection to the coring site in the deeper basin. Snow avalanche detrital material can be integrated into lacustrine sediments in two ways. In the case of a frozen lake, surface avalanche deposits are spread across the ice and subsequently drop to the lake sediment from drifting ice. If an avalanche occurs while the lake is ice-free, the avalanches directly enter into the water, where particles are concentrated in a more restricted area closer to the avalanche corridor. The presence of fine sediment in between gravels could thus be originating from previously deposited particles and/or from the avalanche. Consequently, we consider them as annual sedimentation in our age model. Given that avalanche deposit can be a very local phenomenon, the coring point must be directly beneath the avalanche corridor and thus capture both drop stones and direct avalanche deposits in order to record the maximum number of events. In our record, we identify

an avalanche deposit as multiple gravel elements at the same sediment depth, as opposed to a single element that could be related to a single rock falling from steep slopes. In order to better understand this deposition processes, multiple cores spatially dispersed in the deeper lake basin would give a better overall estimation.

After establishing the age model to the LAU1104A sediment core, we are able to express the gravel abundance per 5 mm slice, for the interval from AD 1880 to present (Fig. 5). The gravel abundance goes from zero to almost 20 gravel elements per 5 mm deposited in the lake floor. A total of 456 gravel elements were identified in the sediment core, 217 of which were identified outside flood layers. Despite this, they represent a total of 106 922 mm^3, constituting 94.9 % of the total measured volume. Gravels found in flood layers are thus characterized by a small size, probably related to lower competence transport mechanism, such as temporary tributaries on the steep slopes only active during a heavy precipitation event. We compared the evolution of gravel number in the annual sedimentation with historic records of winters with higher avalanche activity in the Oisans Valley. The winter of 1922–1923 was an exceptional year in terms of winter precipitation in the Oisans Valley, and avalanches destroyed numerous buildings and covered roads with thick snow deposits (Allix, 1923). The winter of 1969–1970 was also exceptional in terms of heavy snowfall, and no fewer than 800 avalanches were reported. On 10 February 1970, an avalanche killed 39 people, making it the most catastrophic avalanche in the last 200 years (Jail, 1970). In 1978, the Ecrins National Park rangers reported numerous avalanches in the Oisans Valley, especially in spring, with wet-snow avalanches temporarily blocking roads (Ecrins national park internal report, 1978). The avalanche activity in the French Alps has also been explored based on the "Enquête Permanente sur les Avalanches" (EPA) since 1950, which provides historical records of avalanche activity. Based on this record, four periods correspond to higher snow avalanche frequency in the northern French Alps: 1950–1955, 1968–1970, 1978–1988, and 1993–1998 (Eckert et al., 2013; Fig. 5). The most locally representative record of avalanche activity is based on tree ring growth disturbance and identifies 20 events since AD 1919 in the Romanche valley located 10 km north from Lake Lauvitel (Corona et al., 2010; Fig. 5). In the Lake Lauvitel sediment sequence, the periods of increased abundance of rocks are AD 1888, 1898, 1920–1931, 1939, 1949, 1970–1972, 1977–1980 and 1990–1993 (highlighted in blue). Considering our age model uncertainties (Fig. 4), we find that these periods are in rather good agreement with higher avalanche activity from a tree-ring-based calendar probably due to their proximity. Avalanches occur at a local scale (McCollister et al., 2003), but similarity between records was reported at distances as far as 50 km (Butler and Malanson, 1985). In the meantime, the comparison with the EPA record seems more ambiguous. A recent study on tree-ring-based avalanches record tested the representativity of the natural archive to the meteorological conditions during the last 50 years based on the EPA database (Schläppy et al., 2016). It revealed a underestimation compared to natural variability estimated to roughly 60 % (Corona et al., 2012; Schläppy et al., 2014), and may be transferable to lacustrine avalanche deposits. Based on the data comparisons, we propose that intervals of significant avalanche activity in the Oisans Valley are represented by sedimentary layers containing a minimum of four clasts of a >2 mm size present in a 5 mm thickness layer. While this figure remains somewhat speculative and probably non-exhaustive, it may reflect part of avalanche activity deposited in Lake Lauvitel. We thus need to develop both longer-term and multiple site reconstructions of snow avalanche deposits to discuss their variability in terms of forcing mechanism. In these perspectives, the CT scanning method appears to be a very promising tool.

Our X-ray CT-based counting method is well suited for this type of lacustrine sediment because density difference between fine silty and coarse gravel elements is quite significant. The resolution of the CT scan allowed identification of the centimeter-sized gravels found in sediment cores. However, in this study the resolution of the CT scan was limited to a pixel resolution of only 500 µm × 500 µm due to practical constrains. We show that manual and numerical counting were in accordance in the absence of gravel-sized element in the sediment. Additionally, quantitative 3-D imaging proved useful in characterizing gravel size elements that were related to instantaneous deposits. However, smaller clasts were more difficult to discriminate as they were too close to the pixel resolution used. Some discrepancies between the manual and numerical gravel counting have to be noted in our study, which are likely to be an artifact of the image resolution used. This constitutes a limitation of our CT-based technique, but one which could potentially be overcome by using a higher imaging resolution. Similar issues were identified for OM macroremains within the sediment core (Fig.3b-2), which mainly consist of small roots or leaves characterized by an elongated and thin shape. This made them difficult to clearly identify with the CT-scanning resolution applied in this study. However, we could clearly identify the largest OM elements that were located at the base of the thickest flood deposit (Fig. 3b1). This suggests that with further refinements this technique may be used for identifying a suitable depth for sampling of macro-OM constituents for ^{14}C dating. As the analysis is based on relative density, some calibrations of known clastic or organic elements would be necessary in order to enhance qualitative information. Overall, we find that the CT scan is a powerful non-destructive tool for investigating clastic elements in a sedimentary core as well as OM rich levels. It is clear that there is the potential to develop this method, alongside existing techniques, for further applications to a wide range of Quaternary sediment studies.

5 Conclusions

CT scanning is a well-established technique in medical diagnosis and has been used for several geoscience-related studies in recent times. The principle of the analysis is based on differences in the relative densities of an object. This study explores the possibility of using a novel X-ray CT-based approach to analyze distinct deposits in lake sediments. The analysis highlighted the presence of denser >2 mm mineralogical particles in the silty sedimentary matrix, as well as the abundant organic matter which could be a useful tool for sampling macroremains for ^{14}C analysis. Conventional sedimentary analysis coupled with CT scanning of the Lake Lauvitel sediment core facilitated the identification of flood deposits, as well as the presence of poorly sorted layers accompanied with gravel size elements that are thought to be associated with wet-snow avalanches. However, the correspondence between historical and natural archives of data presents some discrepancies. Exploration on both longer timescales and multiple site records would allow for a better understanding of past variability in wet-snow avalanches. The use of the CT scan methodology opens up new possibilities in reconstructing past environmental changes from lacustrine sediments.

Data availability. The grain size data, gravel counts and age model from this study are available at doi:10.1594/PANGAEA.873896 (Fouinat et al., 2017).

Competing interests. The authors declare that they have no conflict of interest.

Acknowledgements. Laurent Fouinat's PhD fellowship was supported by a grant from Ecrins National Park, Communauté des Communes de l'Oisans, Deux Alpes Loisirs and the Association Nationale de la Recherche et de la Technologie (ANRT). The authors wish to thank Ecrins National Park for their authorization for sampling and assistance during the field work. The authors thank the Laboratoire Souterrain de Modane (LSM) facilities for the gamma spectrometry measurements, Hopitaux Universitaires de Genève (HUG) for the CT scan analysis, and Timothy Pollard for correcting the English of this paper.

Edited by: V. Galy
Reviewed by: two anonymous referees

References

Allix, A.: Les avalanches de l'hiver 1922-1923 en Dauphiné, Rev. Géographie Alp. 11, 513–527, doi:10.3406/rga.1923.5519, 1923.

Ancey, C. and Bain, V.: Dynamics of glide avalanches and snow gliding: Glide avlanches and snow gliding, Rev. Geophys., 53, 745–784, doi:10.1002/2015RG000491, 2015.

Appleby, P. G., Richardson, N., and Nolan, P. J.: 241Am dating of lake sediments, in: Environmental History and Palaeolimnology, edited by: Smith, J. P., Appleby, P. G., Battarbee, R. W., Dearing, J. A., Flower, R., Haworth, E. Y., Oldfield, F., and O'Sullivan, P. E., Developments in Hydrobiology. Springer Netherlands, 35–42, 1991.

Arnaud, F., Lignier, V., Revel, M., Desmet, M., Beck, C., Pourchet, M., Charlet, F., Trentesaux, A., and Tribovillard, N.: Flood and earthquake disturbance of 210Pb geochronology (Lake Anterne, NW Alps), Terra Nova, 14, 225–232, 2002.

Arnaud, F., Poulenard, J., Giguet-Covex, C., Wilhelm, B., Révillon, S., Jenny, J.-P., Revel, M., Enters, D., Bajard, M., Fouinat, L., Doyen, E., Simonneau, A., Pignol, C., Chapron, E., Vannière, B., and Sabatier, P.: Erosion under climate and human pressures: An alpine lake sediment perspective, Quaternary Sci. Rev., 152, 1–18, doi:10.1016/j.quascirev.2016.09.018, 2016.

Baker, S. R. and Friedman, G. M.: A non-destructive core analysis technique using X-rays, J. Sediment. Res., 39, 1371–1383, doi:10.1306/74D71E2E-2B21-11D7-8648000102C1865D, 1969.

Bendle, J. M., Palmer, A. P., and Carr, S. J.: A comparison of micro-CT and thin section analysis of Lateglacial glaciolacustrine varves from Glen Roy, Scotland, Quaternary Sci. Rev. 114, 61–77, doi:10.1016/j.quascirev.2015.02.008, 2015.

Blikra, L. H. and Nemec, W.: Postglacial colluvium in western Norway: depositional processes, facies and palaeoclimatic record, Sedimentology, 45, 909–959, doi:10.1046/j.1365-3091.1998.00200.x, 1998.

Bolte, S. and Cordelieres, F. P.: A guided tour into subcellular colocalization analysis in light microscopy, J. Microsc., 224, 213–232, 2006.

Bouma, A. H.: Notes on X-ray interpretation of marine sediments, Mar. Geol., 2, 278–309, 1964.

Butler, D. R. and Malanson, G. P.: A history of high-magnitude snow avalanches, southern Glacier National Park, Montana, USA, Mt. Res. Dev., 175–182, 1985.

Cnudde, V. and Boone, M. N.: High-resolution X-ray computed tomography in geosciences: A review of the current technology and applications, Earth-Sci. Rev., 123, 1–17, doi:10.1016/j.earscirev.2013.04.003, 2013.

Corona, C., Georges, R., Jérôme, L. S., Markus, S., and Pascal, P.: Spatio-temporal reconstruction of snow avalanche activity using tree rings: Pierres Jean Jeanne avalanche talus, Massif de l'Oisans, France, Catena, 83, 107–118, doi:10.1016/j.catena.2010.08.004, 2010.

Corona, C., Saez, J. L., Stoffel, M., Bonnefoy, M., Richard, D., Astrade, L., and Berger, F.: How much of the real avalanche activity can be captured with tree rings? An evaluation of classic dendrogeomorphic approaches and comparison with historical archives, Cold Reg. Sci. Technol., 74, 31–42, 2012.

Dasgupta, P.: Sediment gravity flow – the conceptual problems, Earth-Sci. Rev., 62, 265–281, 2003.

Delunel, R., Hantz, D., Braucher, R., Bourlès, D.L., Schoeneich, P., and Deparis, J.: Surface exposure dating and geophysical prospecting of the Holocene Lauvitel rock slide (French Alps), Landslides, 7, 393–400, doi:10.1007/s10346-010-0221-0, 2010.

Eckert, N., Keylock, C. J., Castebrunet, H., Lavigne, A., and Naaim, M.: Temporal trends in avalanche activity in the French Alps and subregions: from occurrences and runout al-

titudes to unsteady return periods, J. Glaciol., 59, 93–114, doi:10.3189/2013JoG12J091, 2013.

Fouinat, L., Sabatier, P., Poulenard, J., Reyss, J.-L., Montet, X., and Arnaud, F.: A new CT scan methodology to characterize a small aggregation gravel clast contained in a soft sediment matrix, Dataset # 873895, doi:10.1594/PANGAEA.873896, 2017.

Giguet-Covex, C., Arnaud, F., Enters, D., Poulenard, J., Millet, L., Francus, P., David, F., Rey, P.-J., Wilhelm, B., and Delannoy, J.-J.: Frequency and intensity of high-altitude floods over the last 3.5 ka in northwestern French Alps (Lake Anterne), Quaternary Res., 77, 12–22, doi:10.1016/j.yqres.2011.11.003, 2012.

Gilli, A., Anselmetti, F. S., Glur, L., and Wirth, S. B.: Lake sediments as archives of recurrence rates and intensities of past flood events, in: Dating Torrential Processes on Fans and Cones, Springer, 225–242, 2013.

Glur, L., Wirth, S. B., Büntgen, U., Gilli, A., Haug, G.H., Schär, C., Beer, J., and Anselmetti, F. S.: Frequent floods in the European Alps coincide with cooler periods of the past 2500 years, Sci. Rep., 3, 2770, doi:10.1038/srep02770, 2013.

Goldberg, E. D.: Geochronology with 210Pb, Radioact. Dating, 121–131, 1963.

Howard, J. D.: X-ray radiography for examination of burrowing in sediments by marine invertebrate organisms, Sedimentology, 11, 249–258, 1968.

Irmler, R., Daut, G., and Mäusbacher, R.: A debris flow calendar derived from sediments of lake Lago di Braies (N. Italy), Geomorphology, 77, 69–78, doi:10.1016/j.geomorph.2006.01.013, 2006.

Jail, M.: Note sur l'hiver remarquable 1969–1970 dans les Alpes françaises, Rev. Géographie Alp., 58, 505–513, doi:10.3406/rga.1970.3495, 1970.

Jenny, J.-P., Wilhelm, B., Arnaud, F., Sabatier, P., Giguet Covex, C., Mélo, A., Fanget, B., Malet, E., Ployon, E., and Perga, M. E.: A 4D sedimentological approach to reconstructing the flood frequency and intensity of the Rhône River (Lake Bourget, NW European Alps), J. Paleolimnol., 51, 469–483, doi:10.1007/s10933-014-9768-4, 2014.

Jomelli, V. and Bertran, P.: Wet snow avalanche deposits in the French Alps: structure and sedimentology, Geogr. Ann. Ser. Phys. Geogr., 83, 15–28, 2001.

Jomelli, V., Delval, C., Grancher, D., Escande, S., Brunstein, D., Hetu, B., Filion, L., and Pech, P.: Probabilistic analysis of recent snow avalanche activity and weather in the French Alps, Cold Reg. Sci. Technol., 47, 180–192, 2007.

Korup, O. and Rixen, C.: Soil erosion and organic carbon export by wet snow avalanches, The Cryosphere, 8, 651–658, doi:10.5194/tc-8-651-2014, 2014.

Luckman, B.: Drop stones resulting from snow-avalanche deposition on lake ice, J. Glaciol., 14, 186–188, 1975.

Luckman, B.: The geomorphic activity of snow avalanches, Geogr. Ann. A, 31–48, 1977.

McCollister, C., Birkeland, K., Hansen, K., Aspinall, R., and Comey, R.: Exploring multi-scale spatial patterns in historical avalanche data, Jackson Hole Mountain Resort, Wyoming, Cold Reg. Sci. Technol., 37, 299–313, 2003.

Mulder, T. and Alexander, J.: The physical character of subaqueous sedimentary density flows and their deposits, Sedimentology, 48, 269–299, 2001.

Nesje, A., Bakke, J., Dahl, S. O., Lie, O., and Boe, A.-G.: A continuous, high-resolution 8500-yr snow-avalanche record from western Norway, Holocene, 17, 269–277, doi:10.1177/0959683607075855, 2007.

Nielsen, P. R., Dahl, S. O., Jansen, H. L., and Støren, E. N.: Holocene aeolian sedimentation and episodic mass-wasting events recorded in lacustrine sediments on Langøya in Vesterålen, northern Norway, Quaternary Sci. Rev., 148, 146–162, doi:10.1016/j.quascirev.2016.07.011, 2016.

Pirlet, H., Wehrmann, L. M., Brunner, B., Frank, N., Dewanckele, J., Van Rooij, D., Foubert, A., Swennen, R., Naudts, L., Boone, M., Cnudde, V., and Henriet, J.-P.: Diagenetic formation of gypsum and dolomite in a cold-water coral mound in the Porcupine Seabight, off Ireland: Diagenetic gypsum in a cold-water coral mound, Sedimentology, 57, 786–805, doi:10.1111/j.1365-3091.2009.01119.x, 2010.

Postma, G.: Classification for sediment gravity-flow deposits based on flow conditions during sedimentation, Geology, 14, 291–294, 1986.

Reyss, J.-L., Schmidt, S., Legeleux, F., and Bonté, P.: Large, low background well-type detectors for measurements of environmental radioactivity, Nucl. Instrum. Meth. A., 357, 391–397, doi:10.1016/0168-9002(95)00021-6, 1995.

Sæmundsson, T. H., Decaulne, A., and Jónsson, H. P.: Sediment transport associated with snow avalanche activity and its implication for natural hazard management in Iceland, in: International Symposium on Mitigative Measures against Snow Avalanches, 137–142, 2008.

Schläppy, R., Eckert, N., Jomelli, V., Stoffel, M., Grancher, D., Brunstein, D., Naaim, M., and Deschatres, M.: Validation of extreme snow avalanches and related return periods derived from a statistical-dynamical model using tree-ring techniques, Cold Reg. Sci. Technol., 99, 12–26, 2014.

Schläppy, R., Jomelli, V., Eckert, N., Stoffel, M., Grancher, D., Brunstein, D., Corona, C., and Deschatres, M.: Can we infer avalanche–climate relations using tree-ring data? Case studies in the French Alps, Reg. Environ. Change, 16, 629–642, doi:10.1007/s10113-015-0823-0, 2016.

Seierstad, J., Nesje, A., Dahl, S. O., and Simonsen, J. R.: Holocene glacier fluctuations of Grovabreen and Holocene snow-avalanche activity reconstructed from lake sediments in Grningstlsvatnet, western Norway, Holocene, 12, 211–222, doi:10.1191/0959683602hl536rp, 2002.

Sletten, K., Blikra, L. H., Ballantyne, C. K., Nesje, A., and Dahl, S. O.: Holocene debris flows recognized in a lacustrine sedimentary succession: sedimentology, chronostratigraphy and cause of triggering, Holocene, 13, 907–920, doi:10.1191/0959683603hl673rp, 2003.

Støren, E. N., Dahl, S. O., Nesje, A., and Paasche, Ø.: Identifying the sedimentary imprint of high-frequency Holocene river floods in lake sediments: development and application of a new method, Quaternary Sci. Rev., 29, 3021–3033, doi:10.1016/j.quascirev.2010.06.038, 2010.

Sturm, M. and Matter, A.: Turbidites and Varves in Lake Brienz (Switzerland): Deposition of Clastic Detritus by Density Currents, in: Modern and Ancient Lake Sediments, Blackwell Publishing Ltd., 147–168, 1978.

Tins, B.: Technical aspects of CT imaging of the spine, Insights Imaging 1, 349–359, doi:10.1007/s13244-010-0047-2, 2010.

Van Steijn, H.: Stratified slope deposits: periglacial and other processes involved, Geol. Soc. Lond. Spec. Publ., 354, 213–226, doi:10.1144/SP354.14, 2011.

van Steijn, H., Bertran, P., Francou, B., Texier, J.-P., and Hétu, B.: Models for the genetic and environmental interpretation of stratified slope deposits: Review, Permafr. Periglac., 6, 125–146, doi:10.1002/ppp.3430060210, 1995.

Vasskog, K., Nesje, A., Storen, E. N., Waldmann, N., Chapron, E., and Ariztegui, D.: A Holocene record of snow-avalanche and flood activity reconstructed from a lacustrine sedimentary sequence in Oldevatnet, western Norway, Holocene 21, 597–614, doi:10.1177/0959683610391316, 2011.

Weirich, F. H.: Field evidence for hydraulic jumps in subaqueous sediment gravity flows, Nature, 332, 626–629, doi:10.1038/332626a0, 1988.

Wilhelm, B., Arnaud, F., Sabatier, P., Crouzet, C., Brisset, E., Chaumillon, E., Disnar, J.-R., Guiter, F., Malet, E., Reyss, J.-L., Tachikawa, K., Bard, E., and Delannoy, J.-J.: 1400years of extreme precipitation patterns over the Mediterranean French Alps and possible forcing mechanisms, Quaternary Res., 78, 1–12, doi:10.1016/j.yqres.2012.03.003, 2012.

Wilhelm, B., Arnaud, F., Sabatier, P., Magand, O., Chapron, E., Courp, T., Tachikawa, K., Fanget, B., Malet, E., Pignol, C., Bard, E., and Delannoy, J. J.: Palaeoflood activity and climate change over the last 1400 years recorded by lake sediments in the north-west European Alps, J. Quaternary Sci., 28, 189–199, doi:10.1002/jqs.2609, 2013.

Wilhelm, B., Sabatier, P., and Arnaud, F.: Is a regional flood signal reproducible from lake sediments?, Sedimentology, 62, 1103–1117, doi:10.1111/sed.12180, 2015.

Wirth, S. B., Glur, L., Gilli, A., and Anselmetti, F. S.: Holocene flood frequency across the Central Alps – solar forcing and evidence for variations in North Atlantic atmospheric circulation, Quaternary Sci. Rev., 80, 112–128, doi:10.1016/j.quascirev.2013.09.002, 2013.